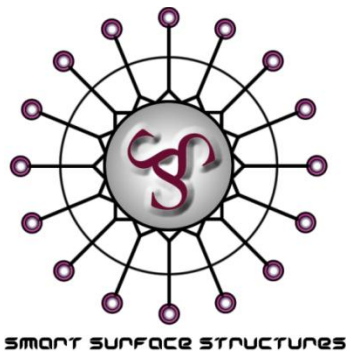


Carbon Nanotubes for Photovoltaic Devices



Thesis submitted to the School of Chemical and Physical Sciences, Faculty of Science
and Engineering, Flinders University in fulfilment of the requirements for the degree of
Doctor of Philosophy

Mark A. Bissett

Declaration

I certify that this thesis does not incorporate without acknowledgment any material previously submitted for a degree or diploma in any university; and that to the best of my knowledge and belief it does not contain any material previously published or written by another person except where due reference is made in the text.

Mark Alexander Bissett

Contents

Declaration.....	i
Contents.....	ii
Acknowledgments	vii
Publications From This Thesis	viii
Abstract.....	x
Figures & Tables	xii
Abbreviations	xxv

Chapter 1

1. Introduction	1
1.0 Power Generation	2
1.1 Photovoltaics.....	3
1.1.1 Silicon Solar Cells	4
1.1.2 Dye Sensitised Solar Cells	6
1.2 Carbon Nanotubes.....	13
1.2.1 Structure of Carbon Nanotubes.....	14
1.2.2 Methods of Carbon Nanotube Production.....	16
1.3 Integration of Carbon Nanotubes in Light Harvesting Technology.....	19
1.3.1 Chemical Modification of Carbon Nanotubes for Light Harvesting Devices ..	23
1.4 Thesis Outline	26

Chapter 2

2. Materials & Methods.....	28
2.0 Experimental Details	29
2.1 Single-walled Carbon Nanotube Solutions.....	29

2.1.1 SWCNT Arrays on Silicon.....	30
2.1.2 Arrays on Fluorine Doped Tin Oxide Coated Glass	31
2.1.3 Carbon Nanotube Electrochemical Solar Cells	32
2.1.4 Multi-walled Carbon Nanotube Devices.....	33
2.2 Chemically Functionalised Single-walled Carbon Nanotube Arrays	33
2.2.1 Ruthenium Tetraphenyl Porphyrin Functionalised Arrays	33
2.2.2 N3 Dye Functionalised Array	36
2.2.3 Dendron Functionalised Array.....	38
2.3 Chemical Vapour Deposition Growth of Carbon Nanotubes	40
2.3.1 Carbon Nanotube Arrays Grown by Chemical Vapour Deposition	40
2.3.2 Carbon Nanotube Arrays Grown by Plasma Enhanced Chemical Vapour Deposition.....	41
2.5 Solar Cell Performance	43
2.5.1 Spectral Response.....	44
2.6 Electrochemistry.....	45
2.6.1 Cyclic Voltammetry.....	45
2.6.2 Differential Pulse Voltammetry	47
2.6.3 Electrochemical Impedance Spectroscopy	49
2.7 Raman Spectroscopy	51
2.8 X-Ray Photoelectron Spectroscopy	54
2.9 Scanning Electron Microscopy	55

Chapter 3

3. Photoresponse of Single-walled Carbon Nanotube Arrays.....	57
3.0 Introduction.....	58
3.1 Characterisation of Carbon Nanotube Array on FTO	59

3.1.1 Raman Spectroscopy of CNT Arrays on FTO	59
3.1.2 XPS Characterisation of SWCNT on FTO	63
3.1.3 Electrochemistry of SWCNT Arrays on FTO	66
3.2 Photovoltaic Properties of Single-Walled Carbon Nanotube Arrays	75
3.2.1 Spectral Response of SWCNT Functionalised FTO.....	83
3.3 Comparison of SWCNT to MWCNT Functionalised FTO.....	85
3.3.1 Raman of MWCNT Functionalised FTO	86
3.3.2 Electrochemistry of MWCNT Functionalised FTO	88
3.3.3 XPS Characterisation of MWCNT Functionalised FTO	91
3.3.4 Photovoltaic Properties of MWCNT Functionalised FTO.....	92
3.4 Chapter Conclusions.....	93

Chapter 4

4. Single-walled Carbon Nanotube Arrays as Scaffolds for Chemical Functionalisation	95
4.0 Introduction.....	96
4.1 Dye Functionalisation of SWCNT Arrays	96
4.1.1 Electrochemical Characterisation of Dye Functionalised SWCNT Arrays.....	96
4.1.2 Photovoltaic Properties of Dye Functionalised SWCNT Arrays	102
4.2 Porphyrin Functionalisation of SWCNT Arrays.....	105
4.2.1 Electrochemical Characterisation of Porphyrin Functionalised SWCNT Arrays.....	106
4.2.2 Photovoltaic Properties of Porphyrin Functionalised SWCNT Arrays	108
4.3 Dendron Functionalisation of SWCNT Arrays	110
4.3.1 Raman Characterisation of Dendron Functionalised SWCNT Arrays	111
4.3.2 Electrochemical Characterisation of Dendron Functionalised SWCNT Arrays.....	112

4.3.3 Photovoltaic Properties of Dendron Functionalised SWCNT Arrays	116
4.4 Dye Modification of Dendron Functionalised SWCNT Arrays	121
4.4.1 Electrochemical Characterisation of Dye Modified Dendron Functionalised SWCNT Arrays	123
4.4.2 Photovoltaic Properties of Dye Modified Dendron Functionalised SWCNT Arrays	129
4.5 Chapter Conclusions	132

Chapter 5

5. Growth of Carbon Nanotubes for Photovoltaic Devices.....	133
5.0 Introduction.....	134
5.1 Thermal Chemical Vapour Deposition Growth of Carbon Nanotube Arrays on Silicon.....	134
5.1.1 Scanning Electron Microscopy of CVD Grown CNT Arrays	135
5.1.2 Electrochemical Characterisation of CVD Grown CNT Arrays	136
5.1.3 Raman Characterisation of CVD Grown CNT Arrays.....	139
5.1.4 XPS Characterisation of CVD Grown CNT Arrays	140
5.1.5 Photovoltaic Properties of CVD Grown CNT Arrays	146
5.2 Thermal Chemical Vapour Deposition Growth of CNT Arrays on Indium Tin Oxide Coated Quartz.....	147
5.2.1 Scanning Electron Microscopy of CVD Grown CNT on ITO Coated Quartz ..	147
5.2.2 Raman Characterisation of tCVD Grown CNT On ITO Coated Quartz	151
5.3 Plasma Enhanced Chemical Vapour Deposition for Growth of Carbon Nanotube Arrays.....	153
5.3.1 Scanning Electron Microscopy.....	155
5.3.2 Electrochemical Characterisation of PECVD Grown CNT Arrays	156
5.3.3 Raman Characterisation of PECVD Grown CNT Arrays.....	158

5.3.4 XPS Characterisation of PECVD Grown CNT Arrays	164
5.3.5 Photovoltaic Properties of PECVD Grown CNT Arrays	166
5.4 Chapter Conclusions	167

Chapter 6

6. Conclusion & Future Work	168
6.1 Conclusions.....	169
6.2 Future Work	171

Chapter 7

7. References.....	173
---------------------------	------------

Acknowledgments

There are many people whose help made this thesis possible and I would like to express my thanks to everyone who has assisted me in this research.

Firstly I should express my thanks and appreciation for my primary supervisor Prof. Joe Shapter, whose ability to reply to questions and queries as well as reading drafts of this thesis in record time has made the process of writing this thesis possible. The wealth of experience you have brought to this project have made it a pleasure to work with you, and I hope that in the future I will be able to continue to collaborate with you as a colleague. I would also like to thank my co-supervisor Assoc. Prof. Jamie Quinton whose insightful input often helped me see what was right in front of me the whole time and whose discussions about PhDs and life in general often helped me put things in perspective.

I especially need to thank the other PhD students within the Smart Surface Structures Group with which I have undertaken this research, both for your professional collaborations and friendship. This includes all members of our research group with specific thanks to Cameron Shearer, Anders Barlow, Adam Blanch, Sam Ogden, Lintern Fairbrother, Leo Velleman, Daniel Tune and Jingxian Yu. I would also like to thank Dr. Ingo Köper for his assistance with the electrochemical analysis and specifically the EIS data interpretation, also Dr. Chris Gibson for his assistance and smooth running of the Raman setup

I would also like to acknowledge the collaboration with the Queensland University of Technology, specifically with Prof. John Bell and his PhD students Paul Moonie and Muthuraaman Achari without whose assistance in establishing our own solar cell testing procedures this work would not have been possible.

I would like to acknowledge the financial support of Flinders University in the form of my Flinders University Research Scholarship and also funding for attending conferences both nationally and internationally.

Lastly, but definitely not least, I would like to thank my whole family for their support throughout this journey. I would especially like to thank my wife Natasha, who has supported and encouraged me throughout this whole process.

Publications From This Thesis

Journal Publications

1. **Bissett, M. A.**; Shapter, J. G., Photocurrent Response from Vertically Aligned Single-Walled Carbon Nanotube Arrays. *J. Phys. Chem. C* 2010, *114* (14), 6778-6783, DOI: 10.1021/jp1003193
2. **Bissett, M. A.**; Shapter, J. G., Electrochemistry and Photocurrent Response from Vertically-Aligned Chemically-Functionalized Single-Walled Carbon Nanotube Arrays. *J. Electrochem. Soc.* 2011, *158* (3), K53-K57, DOI: 10.1149/1.3527057
3. **Bissett, M. A.**, Köper, I., Quinton, J. S., Shapter, J. G., Dendron Growth from Vertically Aligned Single-Walled Carbon Nanotube Thin Layer Arrays for Photovoltaic Devices. *Phys. Chem. Chem. Phys.* 2011, *13*, 6059-6066, DOI: 10.1039/C0CP02740E.
4. **Bissett, M. A.**, Barlow, A. J., Shapter, J. G., Quinton, J. S., Transition from single to multi-walled carbon nanotubes grown by inductively coupled plasma enhanced chemical vapor deposition. *J. Appl. Phys.* 2011, *110* (13), 34301-34306, DOI:10.1063/1.3615945
5. **Bissett, M. A.**, Köper, I., Quinton, J. S., Shapter, J. G., Dye Functionalisation of PAMAM-type Dendrons Grown from Vertically Aligned Single-Walled Carbon Nanotube Arrays for Light Harvesting Antennae. *J. Mater. Chem.* 2011, DOI: 10.1039/C1JM13957F
6. **Bissett, M. A.**, Barlow, A. J., Shearer, C., Quinton, J. S., Shapter, J. G., Carbon Nanotube Modified Electrodes for Photovoltaic Devices. *Carbon*, In Press

Published Conference Proceedings

1. **Bissett, M. A.**, Köper, I.; Shapter, J.G., Photocurrent Response from Vertically Aligned Single-walled Carbon Nanotube Arrays. *Proceedings of the International Conference on Nanoscience and Nanotechnology (ICONN2010)*
2. Shapter, J.G., **Bissett, M. A.**; Photocurrent Response from Vertically-Aligned Chemically-Functionalised Single-walled Carbon Nanotube Arrays. *Proceedings of the International Conference on Nanotechnology: Fundamentals and Applications (ICNFA2010)*
3. **Bissett, M. A.**, Barlow, A. J., Shapter, J. G, Quinton, J. S.; Raman Characterisation of Carbon Nanotubes Grown by Plasma Enhanced Chemical Vapour Deposition. *Proceedings of the Fifth International Conference on Advanced Materials and Nanotechnology (AMN-5)*

Conference Presentations

1. “Photocurrent Response from Vertically Aligned Single-walled Carbon Nanotube Arrays”, International Conference on Nanoscience and Nanotechnology 2010 (ICONN2010), Sydney, NSW, Australia
2. “Electrochemical Impedance Spectroscopy of Chemically Modified Single-Walled Carbon Nanotube Arrays”, ARNAM/ARCNN 2010 Joint Workshop, Adelaide, SA, Australia
3. “Dendrimer Functionalisation of Single Walled Carbon Nanotube Arrays”, 23rd International Microprocesses and Nanotechnology Conference (MNC 2010), Kokura, Fukuoka, Japan
4. “Plasma Enhanced Chemical Vapour Deposition Growth of Single-Walled Carbon Nanotubes”, Fifth International Conference on Advanced Materials and Nanotechnology (AMN-5), 2011, Wellington, New Zealand

Abstract

The aim of this work was to investigate how carbon nanotubes can be applied in the development of novel photovoltaic devices. This has been done by taking an existing system of vertically aligning single-walled carbon nanotubes on oxide surfaces and adapting it to solar cell design. Once the ability to construct solar cells from CNT functionalised electrodes was demonstrated, work then focused on improving the performance of these cells. Initially arrays of vertically aligned SWCNT were used as the working electrode in a DSSC type cell architecture. These CNT solar cells were then characterised by photovoltaic testing. The arrays themselves were investigated using electrochemistry and Raman spectroscopy. It was found that the vertically aligned single walled carbon nanotube arrays were capable of producing a prompt, response times less than 200ms, and stable photocurrent of $\sim 13\mu\text{A}\cdot\text{cm}^{-2}$ and a voltage of 42mV when exposed to $100\text{mW}\cdot\text{cm}^{-2}$ of light. This photoresponse changed with the number of nanotubes attached to the surface and the treatment time used to process the CNTs before attachment. Multi-walled carbon nanotube arrays were also created and analysed and found to be inferior to the SWCNT arrays due to their metallic band structure.

To improve upon the response of the SWCNT arrays they were then chemically modified to increase the cell's performance. This will be done firstly by further functionalising the CNT arrays with chromophores such as N3 dye and ruthenium tetraphenyl porphyrin molecules. Attachment of these redox active molecules was verified by electrochemistry and the surface concentration and electron transfer rates compared to literature and found to be in good agreement. Photovoltaic testing indicated that N3 dye attachment led to an increased photocurrent density ($\sim 17\mu\text{A}\cdot\text{cm}^{-2}$) but a reduced voltage (26mV) when compared to the unmodified array, in agreement with similar work in the

literature. This response could also be modified by altering the attachment of nanotubes to the surface thus altering the resultant dye concentration, with 2 hours of CNT attachment found to produce the maximum dye concentration. Functionalisation was then progressed from simple molecules to PAMAM-type dendrons that were grown from the SWCNT array acting as a core. These dendrons were analysed using electrochemistry, Raman spectroscopy and photovoltaic testing and found to be able to increase performance over the unmodified array by $\sim 70\%$ for the 2nd generation dendron. The two methods of chemical modification were then combined with the dendrons being grown from the SWCNT array and then N3 dye attached to the amine terminated chains. This produced an increased performance over the unmodified dendron with a current density of $\sim 15\mu\text{A}\cdot\text{cm}^{-2}$ whilst maintaining a voltage of 45mV.

To further increase the density of carbon nanotubes on the surface growth of CNTs was undertaken using chemical vapour deposition and then the resultant performance compared to the chemically attached arrays. Growth of nanotubes was undertaken using both thermal and plasma-enhanced procedures. Thermal CVD was found to produce predominantly MWCNT whilst PECVD was able to produce SWCNT. It was found upon comparison of the CVD growth procedure to the covalent attachment that the chemical attachment provided for superior electron transfer kinetics despite lower nanotube coverage. This equated into a superior photoresponse. It was also found that the grown SWCNT were superior to the grown MWCNT, in agreement with previous results which suggested that SWCNT are needed to produce photocurrent due to their semi-conducting nature.

Figures & Tables

Chapter 1

Figure 1.1: AM1.5 solar spectrum (Inset: air mass schematic showing; AM 0, AM 1.0 and AM 1.5), spectrum reproduced from ASTM G173-03. ⁶	4
Figure 1.2: A) Intrinsic silicon B) n-Type silicon with phosphorous dopant C) p-Type silicon with boron dopant. From <i>Sze et al.</i> ⁵	5
Figure 1.3: Energy band diagram of a p-n junction showing photogenerated electron-hole pair. E_v is the valence band energy, E_f the Fermi energy and E_c the conduction band energy. From <i>Sze et al.</i> ⁵	6
Figure 1.4: Schematic of a dye sensitised solar cell showing electronic energy levels. From <i>Calandra et al.</i> ¹³	8
Figure 1.5: Structure of N3 dye molecule.	8
Figure 1.6: J-V curve of DSSC showing key properties. Modified from <i>Grätzel et al.</i> ¹²	9
Figure 1.7: Incident photon to current efficiency for unmodified TiO_2 , and $\text{RuL}'(\text{NCS})_3$ or 'black dye' and $\text{RuL}_2(\text{NCS})_2$ or 'N3' Dyes. From <i>Grätzel et al.</i> ¹⁴	10
Figure 1.8: Examples of alternative dye molecules; Z907, C102 and N749 (From left to right). From <i>Meyer.</i> ²⁰	11
Figure 1.9: Copper complexes used in DSSC electrolyte. From <i>Hattori et al.</i> ²⁸	11
Figure 1.10: Spray coated MWCNT for DSSC counter electrode. Optical image of coated glass slide (a), SEM image of nanotube layer (b). From <i>Ramasamy et al.</i> ³⁶	12
Figure 1.11: ZnO nanowire array based DSSC. From <i>Law et al.</i> ⁴³	12

- Figure 1.12: Integration of SWCNT into existing DSSC. (Left) SEM image showing TiO₂ particles and nanotube composite. (Right) IPCE spectra for TiO₂ and TiO₂/SWCNT mixture. From *Jung et al.*⁴⁶ 13
- Figure 1.13: Graphene sheet (A), single-walled nanotube (B), multi-walled nanotube (C) 14
- Figure 1.14: Transmission electron micrographs of MWCNTS. From *Iijima*.⁶² 14
- Figure 1.15: Schematic showing vectors that produce different chirality CNTs. The vectors OA and OB define the chiral vector *Ch* and the translational vector T of the nanotube, respectively. The rectangle OAB'B defines the unit cell for the nanotube. The figure is constructed for an $(n, m) = (4, 2)$ nanotube. From *Dresselhaus et al.*⁶⁹ 15
- Figure 1.16: Examples of patterned CNT arrays produced by tCVD showing pillars and sheets of dense single-walled carbon nanotubes. From *Hata et al.*⁷² 18
- Figure 1.17: Example of CNT arrays produced by PECVD. From *Meyyappan*.⁸⁵ 19
- Figure 1.18: Response of SWCNT bundles to illumination ($20\text{mW}\cdot\text{cm}^{-2}$) in the presence of a 10V bias. From *Zhang et al.*⁸⁷ 20
- Figure 1.19: SEM image of single nanotube diode (A) Graph of photocurrent produced versus incident light intensity (B). From *Freitag et al.*⁸⁹ 21
- Figure 1.20: Schematic of a SWCNT diode along with I-V curve showing increasing photovoltaic response with increasing illumination intensity. From *Lee*.⁵⁰ 21
- Figure 1.21: Photocurrent and photovoltage on-off cycles for SWCNT film (Incident light $\approx 100\text{mW}\cdot\text{cm}^{-2}$). From *Barazzouk et al.*⁴⁹ 22
- Figure 1.22: Schematic of possible solar cell design and benefits of directed electron transport. From *Kamat*.⁵² 23
- Figure 1.23: Porphyrin molecules used and cell schematic for SWCNT-porphyrin hybrid solar cell. From *Hasobe et al.*⁹² 24

- Figure 1.24: Synthesis of PAMAM dendrimer to generation 0.5 (G-0.5) and a schematic showing the increasing complexity of dendrimer molecules. From *Frechet et al.*¹¹¹25
- Figure 1.25: Schematic of PAMAM dendron growth from MWCNT in solution. From *Pan et al.*⁹⁸26

Chapter 2

- Figure 2.1: Schematic of the hydroxylation of the silicon substrate and subsequent formation of the SWCNT array.31
- Figure 2.2: Schematic of the hydroxylation of the FTO glass substrate and subsequent formation of the SWCNT array.32
- Figure 2.3: Schematic of CNT functionalised electrochemical solar cell architecture. (Not to scale).....33
- Figure 2.4: Schematic of the functionalisation of SWCNT array with RuTPP on FTO Glass. Modified from *Yu et al.*⁹⁴35
- Figure 2.5: Schematic of the functionalisation of SWCNT array with N3 dye on FTO....37
- Figure 2.6: Functionalisation scheme for modifying SWCNTs attached to FTO glass. Step 1: Attachment of PDA leading to G-0.5; Step 2: attachment of methyl acrylate leading to G-1.0. Step 1 and 2 are then alternated for higher generations.39
- Figure 2.7: Schematic of thermal chemical vapour deposition growth of CNTs.41
- Figure 2.8: Reaction chamber used in plasma nanotube growth showing A: top view and B: side view. In B the antenna is shown rotated 90 degrees for clarity. Distance between antenna and sample is 10cm.42
- Figure 2.9: Schematic of PECVD CNT growth process.43
- Figure 2.10: Spectrum of LED solar simulator, from supplier.....44

Figure 2.11: Example cyclic voltammogram with peak current I_p and voltage E_p labelled for both the anodic and cathodic peaks.	46
Figure 2.12: DPV potential waveform E, with respect to time, t. From Manufacturer (BAS Inc).	48
Figure 2.13: Example differential pulse voltammogram with peak current I_p and voltage E_p labelled.....	49
Figure 2.14: Example of EIS spectra, simulated using a Randles type circuit. A) Nyquist Plot. B) Bode Plot.	50
Figure 2.15: Example of equivalent circuits and the corresponding Nyquist plot. Modified from <i>Barsoukov et al.</i> ¹³⁴	50
Figure 2.16: Diagram of Raman spectrometer. Modified from supplier.	52
Figure 2.17: Schematic of an X-ray photoelectron spectrometer.	54
Figure 2.18: XPS spectrum of platinum. Inset: High resolution XPS of Pt 4f binding region.	55
Figure 2.19: Photograph and schematic of a scanning electron microscope.	56

Chapter 3

Figure 3.1: Raman spectra for a single semi-conducting and metallic SWCNT. From <i>Dresselhaus et al.</i> ¹⁴⁶	59
Figure 3.2: Confocal Raman images showing nanotube coverage. (A and B) Image A is a plot of the intensity of the glass specific peak (1030cm^{-1}). Image B is the G band (1570cm^{-1}) intensity present in the spectra (C) for 24 hours of nanotube attachment, with 8 hours cutting time.....	60
Figure 3.3: Graph of D and G ⁺ band ratio and G ⁻ and G ⁺ ratio versus cutting time. Each point represents the average of several individual spectra taken across a wide area on	

the sample, with error bars showing one standard deviation. Dashed line added to guide the eye.....62

Figure 3.4: Histogram of G-band intensity for differing cutting times (2, 4 and 8 hours as indicated) of CNT attached to FTO glass for 24 hours and identical Raman laser intensity.....63

Figure 3.5: XPS survey spectra of bare FTO and SWCNT functionalised FTO.64

Figure 3.6: High resolution XPS spectra of; oxygen 1s binding region (A) and carbon 1s binding region (B) for bare FTO, oxygen 1s binding region (C) and carbon 1s binding region (D) for SWCNT functionalised FTO.....65

Figure 3.7: CV plots for ferrocene in solution with bare FTO working electrode. (A) Graph showing relationship between peak current and square root of scan rate. (B)..67

Figure 3.8: Plot of anodic and cathodic peak potential (E_p) versus the natural logarithm of scan rate (v) for the bare FTO working electrode.68

Figure 3.9: CV plots for ferrocene in solution with SWCNT functionalised working electrode. Scan rate: (innermost) $20\text{mV}\cdot\text{s}^{-1}$, $50\text{mV}\cdot\text{s}^{-1}$, $100\text{mV}\cdot\text{s}^{-1}$, $200\text{mV}\cdot\text{s}^{-1}$, $300\text{mV}\cdot\text{s}^{-1}$, $400\text{mV}\cdot\text{s}^{-1}$, $500\text{mV}\cdot\text{s}^{-1}$ (outermost). (A) Graph showing relationship between peak current and square root of scan rate. (B)69

Figure 3.10: Plot of peak anodic and cathodic potential (E_p) versus the natural logarithm of scan rate (v) for the SWCNT functionalised working electrode.....69

Figure 3.11: Comparison of CV plots for both the bare FTO working electrode and the SWCNT functionalised working electrode at the same scan rate. (Scan rate = $100\text{mV}\cdot\text{s}^{-1}$)70

Figure 3.12: Typical Nyquist plot for a DSSC. Modified From *Wang et al.*¹³⁸71

Figure 3.13: Nyquist plot (A) and Bode plot (C) (without illumination) for a freshly prepared and aged FTO-SWCNT electrochemical solar cells. (B) Shows the enlarged high frequency area. Cells were stored in the dark between testing.....72

Figure 3.14: Platinum symmetrical cell in dark (A). SWCNT symmetrical cell in light (B).	74
Figure 3.15: Equivalent circuits used for electrochemical solar cell modelling.....	74
Figure 3.16: 'Normal' cell Nyquist plot (A) and Bode plot (B) for both measured and simulated data using symmetrical cells.	75
Figure 3.17: On-Off light response from FTO-CNT cell and blank cell containing no CNT. The arrows indicate the light on and off cycle. (CNT attachment time was 24 hours and cutting time was 8 hours. Points are separated by 200ms. Light intensity 35mW.cm^{-2})	76
Figure 3.18: Light soaking response of the cell (From Figure 3.17) left under illumination for over 200 minutes. Dashed line added to show gradual increase in current. Light intensity 35mW.cm^{-2}	77
Figure 3.19: J-V curves for FTO-SWCNT solar cell with incident intensity of 35mW.cm^{-2} and 100mW.cm^{-2}	78
Figure 3.20: J-V curves for a FTO-SWCNT cell under illumination (100mW.cm^{-2}) and darkness.	79
Figure 3.21: Peak current versus CNT attachment time (A). Peak voltage versus CNT attachment time (B). Light intensity is 35mW.cm^{-2}	80
Figure 3.22: Graph of current versus CNT cutting time (A) and voltage versus CNT cutting time. (B) Light intensity is 35mW.cm^{-2} Error bars show 10% experimental error..	81
Figure 3.23: Wavelength response of FTO-SWCNT solar cell along with UV-Vis absorption spectrum of SWCNT solution.....	84
Figure 3.24: Spectral response of FTO-SWCNT solar cells of different SWCNT cutting times. (A) Photovoltage, (B) photocurrent density and (C) power output.....	85

- Figure 3.25: SEM images of CNT modified surfaces. (A-B) MWCNT attached to FTO, (C-D) SWCNT attached to FTO.86
- Figure 3.26: Raman spectra comparing SWCNT and MWCNT chemically attached to FTO (A). Enlargement of G band region (B).87
- Figure 3.27: CV Plots for ferrocene in solution with MWCNT functionalised working electrode. (A) Graph showing relationship between peak current and square root of scan rate. (B)88
- Figure 3.28: Plot of anodic and cathodic peak potential (E_p) versus the natural logarithm of scan rate (ν) for the MWCNT functionalised working electrode.89
- Figure 3.29: Comparison of CV plots for bare FTO, SWCNT and MWCNT functionalised FTO, along with a table summarising these values.....90
- Figure 3.30: XPS survey spectra for bare FTO and MWCNT functionalised FTO.91
- Figure 3.31: High resolution XPS of O1s (A) and C1s Regions (B) for FTO-MWCNT.92
- Figure 3.32: J-V curve comparison for MWCNT and SWCNT solar cells, along with tabulated J_{sc} , V_{oc} and power values.93

Chapter 4

- Figure 4.1: DPV of unmodified and N3 modified CNT arrays (24 Hours attachment time). DPV of N3 in solution (Inset).....97
- Figure 4.2: N3 peak current vs. CNT exposure time on silicon. (Dashed line added to guide the eye)98
- Figure 4.3: DPV comparison of N3 functionalised SWCNT arrays on both silicon and FTO substrates.....99
- Figure 4.4: Background subtracted cyclic voltammograms of FTO-CNT-EDA-N3 (2hr SWCNT attachment time). (A) Graph of peak current versus scan rate. (B)100

- Figure 4.5: Plot of anodic and cathodic peak potential (E_p) versus $\ln(v)$ for N3 functionalised SWCNT on FTO. 102
- Figure 4.6: J-V comparison between SWCNT and N3 functionalised SWCNT cells. (A) J-V comparison of 2 and 24 hour attachment times for N3-SWCNT cells. (B) Light intensity is $35\text{mW}\cdot\text{cm}^{-2}$ 104
- Figure 4.7: On-Off light response for 24Hr CNT modified with N3. (A) On-Off light response for unmodified 24Hr CNT produced at similar time (B) Light intensity $35\text{mW}\cdot\text{cm}^{-2}$ 105
- Figure 4.8: Cyclic voltammograms of RuTTP in CH_2Cl_2 . Dashed line is the background subtracted trace showing two reversible oxidation peaks. 106
- Figure 4.9: Background subtracted DPV of RuTTP functionalised SWCNT array for 2hrs and 24 hrs of SWCNT attachment. 108
- Figure 4.10: Comparison of the J-V Curves for RuTTP functionalised cells with 2 and 24 hours of SWCNT attachment. Light intensity $35\text{mW}\cdot\text{cm}^{-2}$ 109
- Figure 4.11: Comparison of the J-V curves from RuTTP and N3 functionalised cells. (Both cells used 2 hours of SWCNT attachment) 110
- Figure 4.12: Normalised Raman spectra for the G-0.5 and G-2.0 modified surface. The graphitic or G band and the disorder or D band are labelled. 112
- Figure 4.13: DPV of p-phenylenediamine solution and G-0.5 modified SWCNT. 113
- Figure 4.14: Background subtracted DPV for G-0.5 and G-2.0 modified array. Plot of peak voltage and FWHM versus dendron generation. (Inset) 114
- Figure 4.15: Bode plots for the different dendron generations. Solid lines correspond to fit using an equivalent circuit. 115
- Figure 4.16: (A) Plot comparing DPV peak height and photoresponse. (B) Plot comparing EIS resistance and photoresponse. (C) Plot comparing EIS capacitance and

photoresponse. Error bars are from fitting of equivalent circuit and smoothed line present to guide the eye.....117

Figure 4.17: J-V curve for the unmodified SWCNT array (G-0.0) and the 2nd generation dendron modified array (G-2.0). Light intensity 100mW.cm⁻². Also included are the dark current curves with no illumination.118

Figure 4.18: Spectral response of unmodified SWCNT cell (G-0.0) as seen in Chapter 3 and UV-Vis of SWCNT in solution. (A) Response of the dendron modified cell (G-2.0 and G-2.5) and the UV-Vis of the dendrimer in solution. (B)120

Figure 4.19: Schematic of N3 dye modification of successive generations of dendron.122

Figure 4.20: DPV comparison of different generations of N3 modified dendrons. Dashed line is DPV for N3 in solution.124

Figure 4.21: Background subtracted cyclic voltammograms with increasing scan rate for G-1.5-N3 modified substrate. (A) Plot of peak current versus scan rate from CV plots. (B) Plot of peak voltage versus the natural log of scan rate. (C)125

Figure 4.22: Bode (A) and Nyquist (B) plots for G-1.5 and G-1.5-N3 electrochemical solar cells under illumination. Dashed line represents fit from an equivalent circuit diagram.128

Figure 4.23: Comparison of J-V curves for G-1.5 and G-1.5-N3 modified SWCNT array. (A) J-V curves for successive generations of N3 modified dendrons. (B) Light intensity is 100mW.cm⁻².....130

Figure 4.24: Trend for DPV peak current and photocurrent for N3 modified dendrons.131

Chapter 5

Figure 5.1: SEM images of tCVD grown CNT array on silicon.135

Figure 5.2: tCVD CNTs grown with a nickel catalyst.	136
Figure 5.3: CV plots for ferrocene in solution with bare silicon working electrode. (A) Graph showing relationship between peak current and square root of scan rate. (B)	137
Figure 5.4: CV plots for ferrocene in solution with tCVD functionalised working electrode. (A) Graph showing relationship between peak current and square root of scan rate. (B)	137
Figure 5.5: Comparison of CV plots for bare silicon and tCVD grown CNT on silicon at an identical scan rate ($100\text{mV}\cdot\text{s}^{-1}$).....	138
Figure 5.6: Plot of anodic and cathodic peak potential (E_p) versus the natural logarithm of scan rate (v) for the tCVD functionalised working electrode.	139
Figure 5.7: Comparison between tCVD grown SWCNT arrays and purchased MWCNT arrays chemically attached to FTO glass.	140
Figure 5.8: XPS survey spectrum of bare silicon.	141
Figure 5.9: XPS survey spectrum of silicon after 5nm iron deposition.	142
Figure 5.10: High resolution XPS spectrum of oxygen 1s binding region for silicon after iron catalyst layer deposition.....	143
Figure 5.11: Survey XPS spectrum of tCVD MWCNT surface.	144
Figure 5.12: High resolution XPS spectra of O1s binding region (A) and C1s binding region (B) for the tCVD MWCNT surface.	145
Figure 5.13: XPS spectra comparing each step of tCVD CNT growth.....	146
Figure 5.14: J-V curve for tCVD grown and chemically attached MWCNT. Light intensity $100\text{mW}\cdot\text{cm}^{-2}$	147

- Figure 5.15: SEM images of ITO coated quartz slides. A) As received and B) after 750°C for 10 mins. 148
- Figure 5.16: Angled SEM image of tCVD Modified ITO-quartz slide showing iron-no iron interface. (A) Zoom of single sphere on no iron side. (B) Zoom of single sphere on iron side. (C)..... 149
- Figure 5.17: EDX spectrum of spheres seen on ITO surface. 150
- Figure 5.18: Side-on view of CNTs grown on ITO-quartz..... 150
- Figure 5.19: SEM images of CNTs grown on ITO without hydrogen..... 151
- Figure 5.20: Raman image (G-Band) of CNT covered sphere. (A) SEM image of a similar CNT covered sphere. (B) 152
- Figure 5.21: Raman spectra of the tCVD CNTs grown on ITO-quartz. 153
- Figure 5.22: Scanning electron microscopy images of the patterned substrate after CNT growth at different magnifications. The scale bars are 500 μm (A), 50 μm (B), 10 μm (C) and 2 μm (D). 155
- Figure 5.23: Comparison of CV plots for bare silicon, tCVD and PECVD grown CNT on silicon at identical scan rates (100mV.s⁻¹)..... 156
- Figure 5.24: CV plots for ferrocene in solution with PECVD functionalised working electrode. (A) Graph showing relationship between peak current and square root of scan rate. (B) 157
- Figure 5.25: Plot of anodic and cathodic peak potential (E_p) versus the natural logarithm of scan rate (v) for the PECVD functionalised working electrode..... 157
- Figure 5.26: Raman spectra corresponding to the patterned area (SWCNT) and unpatterned area (Silicon). Inset is a 100x100 μm image plotting the intensity of the G band at 1590cm⁻¹ showing the boundary between where the masked areas. 159

Figure 5.27: Enlargement of Raman G Band region showing G^- peak at 1570cm^{-1} and G^+ peak at 1590cm^{-1} , characteristic of semi-conducting SWCNT.....	160
Figure 5.28: Raman spectra with changing growth time (A) and growth temperature (B).	162
Figure 5.29: Raman spectra for nickel and iron catalysts showing D and G Bands (A). Spectra for aluminium underlay present and no aluminium layer. (B)	163
Figure 5.30: XPS survey spectra for bare silicon, silicon after iron deposition and finally after PECVD growth has occurred.....	164
Figure 5.31: High resolution XPS spectrum of C1s binding region.	165
Figure 5.32: J-V curves for PECVD grown SWCNT electrode and chemically attached SWCNT electrode. Light intensity $100\text{mW}\cdot\text{cm}^{-2}$	166
Figure 5.33: J-V curves for PECVD grown SWCNT electrode and tCVD MWCNT electrode. Light intensity $100\text{mW}\cdot\text{cm}^{-2}$	167

Tables

Chapter 1

Table 1.1: Comparison between carbon nanotubes and silicon. Modified from <i>Zhu et al.</i> ⁵⁹	16
---	----

Chapter 2

Table 2.1: List of wavelength filters used in this work.....	44
Table 2.2: Raman spectral features of carbon nanotubes with laser energy 2.41eV. Modified from <i>Dresselhaus et al.</i> ⁶⁹	53

Chapter 3

Table 3.1: Frequency (f) and effective electron lifetime (τ_{eff}) for fresh and aged cells..	73
Table 3.2: Integrated area under histogram peaks from Figure 3.4, and current from Figure 3.22.....	82
Table 3.3: Raman D/G ratio for SWCNT and MWCNT modified FTO.....	88

Chapter 4

Table 4.1: Comparison of redox active molecules chemically attached to SWCNT arrays.	101
Table 4.2: Surface concentration and electron transfer coefficients of N3 dye for successive dendron generations.....	127
Table 4.3: Summary of resistance and capacitance values produced by fitting an equivalent circuit model to the data shown in Figure 4.22.	129
Table 4.4: Photocurrent, photovoltage and total power for N3 modified surfaces.....	131

Chapter 5

Table 5.1: Methane dissociation reactions. From <i>Mao et al.</i> ⁸³	154
---	-----

Abbreviations

4-Aminopyridine	4-AP
Air Mass	AM
Acetylene	C ₂ H ₂
Counter Electrode	CE
Methane	CH ₄
Carbon Nanotube	CNT
Constant Phase Element	CPE
Cyclic Voltammetry	CV
Chemical Vapour Deposition	CVD
Disorder Raman Band	D-Band
N,N'-Dicyclohexylcarbodiimide	DCC
Dichloromethane	DCM
De-Ionised	DI
4-Dimethylaminopyridine	DMAP
N,N-Dimethylformamide	DMF
Dimethyl Sulfoxide	DMSO
Density of States	DOS
Differential Pulse Voltammetry	DPV
Dye Sensitised Solar Cell	DSSC
Ethylenediamine	EDA
Energy Dispersive X-ray Analysis	EDX
Electrochemical Impedance Spectroscopy	EIS
Peak Potential	E _p
Fill Factor	<i>ff</i>
Fluorine Doped Tin Oxide	FTO
Full Width Half Maximum	FWHM
Graphitic Raman Band	G-Band
Hydrogen Peroxide	H ₂ O ₂
Sulphuric Acid	H ₂ SO ₄
Nitric Acid	HNO ₃
Iodide/Tri-iodide	I ⁻ /I ₃ ⁻

Inductively Coupled Plasma	ICP
Incident Photon to Current Efficiency	IPCE
Indium Tin Oxide (In ₂ O ₃ 90% - SnO ₂ 10%)	ITO
Current-Voltage	I-V
Short Circuit Current Density	J_{sc}
Current Density-Voltage	J-V
Electron Transfer Co-efficient	k_s
Multi-Walled Carbon Nanotube	MWCNT
<i>cis</i> -bis(isothiocyanato)bis(2,2'-bipyridyl-4,4'-dicarboxylato)-ruthenium(II)	N3
Poly(amidoamine)	PAMAM
P-Phenylenediamine	PDA
Plasma Enhanced Chemical Vapour Deposition	PECVD
Radial Breathing Mode	RBM
Reference Electrode	RE
Ruthenium Tetrphenyl Porphyrin	RuTPP
Standard Cubic Centimetres per Minute	SCCM
Scanning Electron Microscopy	SEM
Single-Walled Carbon Nanotube	SWCNT
Tetrabutylammonium Hexafluorophosphate	TBAPF ₆
Thermal Chemical Vapour Deposition	tCVD
Transmission Electron Microscopy	TEM
Titanium Dioxide, Titania	TiO ₂
Ultra-Violet-Visible Light Spectroscopy	UV-Vis
Open Circuit Voltage	V_{oc}
Working Electrode	WE
X-ray Photoelectron Spectroscopy	XPS
Real Component of Impedance	Z'
Imaginary Component of Impedance	Z''
Global Efficiency	η
Scan Rate	ν
Raman Frequency	ω